Influence of shell compressibility on the ultrasonic properties of polydispersed suspensions of nanometric encapsulated droplets

Matthieu Guédra,[a] Tony Valier-Brasier, Jean-Marc Conoir, and François Coulouvrat
Sorbonne Universités, UPMC Université Paris 06, CNRS UMR 7190, Institut Jean Le Rond d'Alembert, F-75005 Paris, France

Ksenia Astafyeva and Jean-Louis Thomas
Sorbonne Universités, UPMC Université Paris 06,CNRS UMR 7588, Institut des NanoSciences de Paris, F-75005 Paris, France

(Received 16 September 2013; revised 19 December 2013; accepted 27 January 2014)

Liquid droplets of nanometric size encapsulated by a polymer shell are envisioned for targeted drug delivery in therapeutic applications. Unlike standard micrometric gas-filled contrast agents used for medical imaging, these particles present a thick shell and a weakly compressible core. Hence, their dynamical behavior may be out of the range of validity of the models available for the description of encapsulated bubbles. In the present paper, a model for the ultrasound dispersion and absorption in a suspension of nanodroplets is proposed, accounting for both dilatational and translational motions of the particle. The radial motion is modeled by a generalized Rayleigh–Plesset-like equation which takes into account the compressibility of the viscoelastic shell, as well as the one of the core. The effect of the polydispersity of particles in size and shell thickness is introduced in the coupled balance equations which govern the motion of the particles in the surrounding fluid. Both effects of shell compressibility and polydispersity are quantified through the dispersion and absorption curves obtained on a wide ultrasonic frequency range. Finally, some results for larger gas-filled particles are also provided, revealing the limit of the role of the shell compressibility.
 [http://dx.doi.org/10.1121/1.4864784]

PACS number(s): 43.20.Hq, 43.35.Bf, 43.80.Sh [NAG] Pages: 1044–1055

I. INTRODUCTION

Propagation of acoustic waves in a dilute suspension is of interest in many situations and in particular to characterize colloidal dispersions or suspensions.[1] The main technique of characterization, acoustic spectroscopy, consists in measuring the speed of sound and attenuation of the solution as a function of the frequency. These measurements are compared to a model to infer some of the physical properties of the mixture that enter the model as parameters. The first problem is the modeling of the scattering of the incident wave by a particle. For large spherical particles and an incident plane wave, the solution in linear regime is provided by the so-called ECAH theory[2,3] (named after its authors Epstein, Carhart, Allegra, and Hawley). The second problem comes from the multiple scattering that must be taken into account.[4] When the solution is sufficiently dilute, the independent scattering approximation is used.[5] An alternative approach is the coupled phase theory[6] that provides dispersion relation for small spherical particles. All these works are related to the characterization of mixture and are concerned by the linear response of the particles only. The acoustical behavior of suspensions is also of interest for medical applications for which contrast agents are developed. In this last case, the scattering particle is an elastic spherical shell with gaseous core. Even for diagnostic, the nonlinear response of the scatterer is crucial to the application and the dilatational mode is dominant. To mitigate this difficulty, models based on different versions of the Rayleigh–Plesset equation were developed.[7] However, the therapeutic applications of gaseous contrast agents are limited by their micrometric size that prevents extravasation and their short lifetime that strongly hinders the possibility of targeting specific tissue.[8] New kinds of contrast agents are under development,[9–11] with radii around hundred nanometers, a liquid core and a relatively thick shell made of either polymers or surfactants. New models are therefore needed for the acoustical behavior of these objects. A previous model[12] for monodisperse suspensions is based on a coupled phase theory combining Church's model[13] for the dilatational mode and Faxén formula[14,15] for the viscous-inertial translational mode. These two modes were found of comparable amplitude for these contrast agents. Here we extend the range of validity of this model, first by modifying Church's model to take into account the compressibility of the shell, and second by modeling the double polydispersity both in particle size and shell thickness. In Sec. II, the equations governing the radial motion of one single particle excited by an external pressure field are derived. These equations are a generalization of the Rayleigh–Plesset equation for a viscoelastic compressible shell in a slightly compressible liquid. The effect of the shell compressibility is captured in a single parameter whose dependence with frequency and

[a]Author to whom correspondence should be addressed. Electronic mail: matthieu.guedra@dalembert.upmc.fr

shell properties is studied (Sec. III). Then, the balance equations accounting for the polydispersity of the particles are given (Sec. IV) and the linear dispersion relation for a harmonic plane wave is obtained (Sec. V). The effects of compressibility and polydispersity are quantified in Sec. VI through the dispersion and absorption curves provided for nanometric encapsulated droplets, as well as for standard gas-filled contrast agents.

II. DYNAMICS OF THE PARTICLE

The particle (Fig. 1) is constituted of a shell with inner radius R_1 and outer radius R_2 containing a liquid or solid core of mass density ρ^c and speed of sound c^c (compression waves). The shell is immersed into a compressible, Newtonian fluid, with mass density ρ, speed of sound c, shear viscosity μ, and bulk viscosity ζ.

A. Surrounding fluid

The model is restricted to the case of incident acoustic waves such that the acoustic wavelength in the ambient liquid is very large compared to the radius of the particle, a very well satisfied assumption for particles of nano or micrometric size and for medical ultrasound frequencies (1–10 MHz). In these conditions, the ambient liquid may be considered as almost incompressible in a layer close to the particle. This situation is the one encountered in the derivation of Rayleigh–Plesset equations for gas bubbles in a liquid. Here we use the Keller–Kolodner equation[16] which accommodates for weak compressibility of the ambient fluid (dot denotes time derivative):

$$R_2\ddot{R}_2\left(1-\frac{\dot{R}_2}{c}\right)+\frac{3}{2}\dot{R}_2^2\left(1-\frac{\dot{R}_2}{3c}\right) = \left(1+\frac{\dot{R}_2}{c}\right)H+\frac{R_2}{c}\dot{H}, \tag{1}$$

where the function $H(t)$ is given by

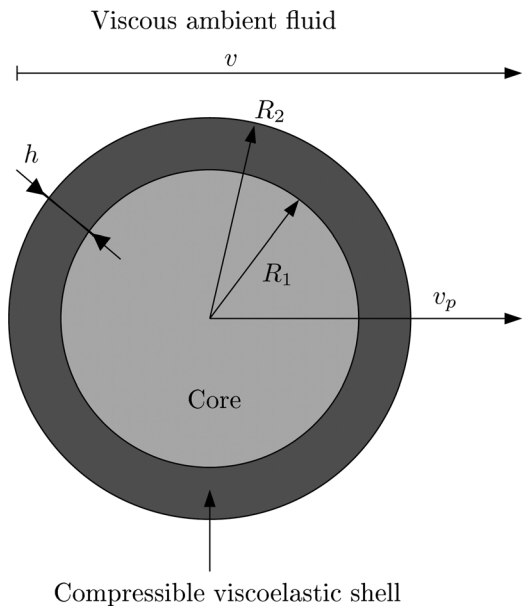

FIG. 1. Schematic drawing of one encapsulated droplet.

$$H(t)=\frac{1}{\rho}\left[p(R_2)-p_\infty\right]. \tag{2}$$

These equations require to know the pressures at both boundaries, i.e., the pressure p in the liquid at the outer interface $r=R_2$, and the pressure p_∞ far from the particle. For this last one, at a distance comparable to the wavelength, the ambient liquid is weakly compressible and the pressure p_∞ is simply the sum of the ambient pressure p_0 and the acoustic pressure. Then, only the pressure at the particle outer interface is needed to close the model.

Another equivalent convenient form of this equation is obtained using once again the assumption of weak compressibility of the ambient liquid. At first order (incompressible) $H=R_2\ddot{R}_2+3\dot{R}_2^2/2$, and substituting this into Eq. (1) yields[17,18]

$$R_2\ddot{R}_2+\frac{3}{2}\dot{R}_2^2-\frac{1}{c}\left(R_2^2\dddot{R}_2+6R_2\dot{R}_2\ddot{R}_2+2\dot{R}_2^3\right)=H. \tag{3}$$

B. Radial velocity in the particle

We consider spherical deformations with radial velocity $\mathbf{v}^{c,s}=v^{c,s}(r)\mathbf{e_r}$, where r is the radial coordinate and where indices c and s relate to the core and to the shell, respectively. Moreover, the size of the particle being much smaller than the acoustic wavelength, the densities $\rho^{c,s}$ can be considered as spatially uniform in the particle. Therefore, the conservation of mass in the particle yields

$$\frac{1}{r^2}\frac{\partial(r^2v^{c,s})}{\partial r}=-\frac{1}{\rho^{c,s}}\frac{\partial\rho^{c,s}}{\partial t}=-\frac{\dot{\rho}^{c,s}}{\rho^{c,s}}. \tag{4}$$

Because there are no matter exchanges between the shell and its surroundings, the total mass of each medium $m^{c,s}=\rho^{c,s}V^{c,s}$ does not vary with time so that

$$-\frac{\dot{\rho}^{c,s}}{\rho^{c,s}}=\frac{\dot{V}^{c,s}}{V^{c,s}}=3\dot{A}^{c,s}, \tag{5}$$

where $\dot{A}^{c,s}$ is a function of time only. Integrating Eq. (4) with the help of Eq. (5) leads to the following expression for the velocity fields in the shell and in the core:

$$v^{c,s}=r\dot{A}^{c,s}+\frac{\dot{B}^{c,s}}{r^2}. \tag{6}$$

Equation (6) is the general expression for a quasi-static velocity field with spherical symmetry. Such expression is recovered because the size of the particle is much smaller than the acoustic wavelength. From Eq. (5), functions $\dot{A}^{c,s}$ are easily computed,

$$\dot{A}^s=\frac{R_2^2\dot{R}_2-R_1^2\dot{R}_1}{R_2^3-R_1^3}, \tag{7}$$

$$\dot{A}^c=\frac{\dot{R}_1}{R_1}. \tag{8}$$

Functions $\dot{B}^{c,s}$ are determined on the one hand, from the boundary conditions $v^s(R_2)=\dot{R}_2$ for the normal velocity at

the outer interface and, on the other hand, from the condition that the velocity at center $v^c(r=0)$ should remain finite and even cancel by symmetry,

$$\dot{B}^s = \frac{R_1^2 R_2^2 (R_2\dot{R}_1 - R_1\dot{R}_2)}{R_2^3 - R_1^3}, \tag{9}$$

$$\dot{B}^c = 0. \tag{10}$$

Note that the derivation of Rayleigh–Plesset equation is based on the same procedure applied to the embedding liquid. In this well-known case,[19] starting from the quasi-static hypothesis, Eq. (6), and requiring a finite velocity at infinity leads to $\dot{A}=0$. This is equivalent to the assumption of incompressibility, i.e., $\dot{V}^{c,s}=0$. Then as above, the constant $\dot{B}=R_2^2\dot{R}_2$ is fixed by the continuity of the normal velocity at $r=R_2$. The same idea was followed by Church[13] but he also used the incompressible hypothesis for the shell leading to $\dot{A}^s=0$. This last hypothesis is more restrictive than uniformity of density or pressure used in Eq. (4) which is valid as long as the dynamics is slow compared to the speed of sound inside the particle. While incompressibility is a valid assumption for thin walled bubble, we will see that this is not true for thick shells or for a shell and a core with comparable compressibilities. This last situation is the one encountered in nanometric contrast agents that are the subject of this work.

C. Stresses in the particle

We assume that the materials of the shell and of the core behave as viscoelastic isotropic materials following an instantaneously relaxing rheology of the Kelvin–Voigt type. In this linear approximation for constitutive laws of the shell material, and due to the spherical symmetry and to the radial motion of the particle, the normal stress,

$$\sigma_{rr}^{s,c}(r,t) = \epsilon_{rr}^{s,c}(r,t) + \tau_{rr}^{s,c}(r,t), \tag{11}$$

is written as the sum of an elastic part $\epsilon_{rr}^{s,c}$ and a viscous part $\tau_{rr}^{s,c}$, respectively related to the normal displacement $u^{s,c}$ and velocity $v^{s,c}$,

$$\epsilon_{rr}^{s,c}(r,t) = K^{s,c}\left(\frac{\partial u^{s,c}}{\partial r} + \frac{2u^{s,c}}{r}\right) + \frac{4}{3}G^{s,c}\left(\frac{\partial u^{s,c}}{\partial r} - \frac{u^{s,c}}{r}\right), \tag{12a}$$

$$\tau_{rr}^{s,c}(r,t) = \zeta^{s,c}\left(\frac{\partial v^{s,c}}{\partial r} + \frac{2v^{s,c}}{r}\right) + \frac{4}{3}\mu^{s,c}\left(\frac{\partial v^{s,c}}{\partial r} - \frac{v^{s,c}}{r}\right). \tag{12b}$$

In Eqs. (12), $K^{s,c}$ and $G^{s,c}$ are instantaneous bulk and shear moduli and $\zeta^{s,c}$ and $\mu^{s,c}$ are bulk and shear viscosities, respectively. Replacing Eq. (6) for the velocity field in Eq. (12b) directly yields the expression of the viscous part of the stress tensor $\tau_{rr}^{s,c}$,

$$\tau_{rr}^{s,c}(r,t) = 3\zeta^{s,c}\dot{A}^{s,c} - 4\mu^{s,c}\frac{\dot{B}^{s,c}}{r^3}. \tag{13}$$

Noting the similarity between the expression of the viscous and elastic stress, Eqs. (12), the time derivative of the elastic stress is easily obtained,

$$\frac{\partial \epsilon_{rr}^{s,c}(r,t)}{\partial t} = 3K^{s,c}\dot{A}^{s,c} - 4G^{s,c}\frac{\dot{B}^{s,c}}{r^3}. \tag{14}$$

It is interesting to note that the bulk contributions are uniform as expected from the quasi-static assumption. It is worth noting that because an analytical expression of the integral of $\dot{B}^s$ cannot be found, we are not able to derive an explicit expression of the elastic stress valid everywhere in the shell. Nevertheless, it can be easily demonstrated that $\dot{B}^s$ may be written from Eq. (9) under the two following equivalent forms:

$$3\dot{B}^s = \frac{d}{dt}\left(R_1^3\right) - R_1^3\frac{d}{dt}\left[\ln\left(R_2^3 - R_1^3\right)\right], \tag{15a}$$

$$3\dot{B}^s = \frac{d}{dt}\left(R_2^3\right) - R_2^3\frac{d}{dt}\left[\ln\left(R_2^3 - R_1^3\right)\right]. \tag{15b}$$

Thus, the last term appearing in the right-hand side of Eq. (14) is expressed at both interfaces from Eqs. (15):

$$\frac{\dot{B}^s(t)}{R_1^3} = -\frac{1}{3}\frac{d}{dt}\left[\ln\left(\frac{R_2^3 - R_1^3}{R_1^3}\right)\right], \tag{16a}$$

$$\frac{\dot{B}^s(t)}{R_2^3} = -\frac{1}{3}\frac{d}{dt}\left[\ln\left(\frac{R_2^3 - R_1^3}{R_2^3}\right)\right]. \tag{16b}$$

The integration of Eqs. (16) is straightforward and the elastic stresses at both interfaces are then obtained,

$$\epsilon_{rr}^s(R_1) = K^s\ln\left(R_2^3 - R_1^3\right) + \frac{4}{3}G^s\ln\left(\frac{R_2^3 - R_1^3}{R_1^3}\right) + C_1^s, \tag{17a}$$

$$\epsilon_{rr}^s(R_2) = K^s\ln\left(R_2^3 - R_1^3\right) + \frac{4}{3}G^s\ln\left(\frac{R_2^3 - R_1^3}{R_2^3}\right) + C_2^s, \tag{17b}$$

$$\epsilon_{rr}^c(r) = K^c\ln(R_1^3) + C_1^c, \tag{17c}$$

where C_1^s, C_2^s, and C_1^c are arbitrary constants which can be determined by the interfacial stresses at the static equilibrium. In the following, we do not consider any prestressed configuration and we neglect the effects of surface tensions. For the investigated nanodroplets,[9–11] surface tensions values are unknown. For typical values around $0.1\,\mathrm{N\,m^{-1}}$, their influence is at least one order of magnitude smaller than elasticity and has been shown to simply increase the shell rigidity.[12] Therefore at equilibrium, $R_1 = R_{10}$, $R_2 = R_{20}$, $\dot{R}_1 = \dot{R}_2 = 0$, and the stress is given by ambient pressure p_0. Thus setting, the expressions of the normal stresses at each interface are

$$\sigma_{rr}^s(R_1) = -p_0 + K^s\ln\left(\frac{R_2^3 - R_1^3}{R_{20}^3 - R_{10}^3}\right) + \frac{4}{3}G^s\ln\left(\frac{R_{10}^3}{R_1^3}\frac{R_2^3 - R_1^3}{R_{20}^3 - R_{10}^3}\right) + 3\zeta^s\dot{A}^s - 4\mu^s\frac{\dot{B}^s}{R_1^3}, \tag{18a}$$

$$\sigma^s_{rr}(R_2) = -p_0 + K^s \ln\left(\frac{R_2^3 - R_1^3}{R_{20}^3 - R_{10}^3}\right) + \frac{4}{3}G^s \ln\left(\frac{R_{20}^3}{R_2^3}\frac{R_2^3 - R_1^3}{R_{20}^3 - R_{10}^3}\right) + 3\zeta^s \dot{A}^s + 4\mu^s \frac{\dot{B}^s}{R_2^3}, \tag{18b}$$

$$\sigma^c_{rr}(R_1) = -p_0 + K^c \ln\left(\frac{R_1^3}{R_{10}^3}\right) + 3\zeta^c \dot{A}^c. \tag{18c}$$

It is worth noting that, for the core, the shear moduli play no role and the elastic medium can be considered as a fluid. In this particular case and in the framework of linear oscillations, it is convenient to introduce the speed of sound of bulk waves in the core, so that $K^c = \rho^c c^{c2}$. Note also that in the case of an incompressible shell, the function $\dot{A}^s$ is zero and one has $R_2^3 - R_1^3 = R_{20}^3 - R_{10}^3$, thus leading to expressions for the normal stresses which depend only on the shear moduli.

D. Generalized Rayleigh–Plesset equations

Since the divergence of the viscous tensor vanishes for spherical radial particle velocity in an incompressible medium, the Navier–Stokes equation reduces to the Euler equation. Therefore viscosity does not appear in Eq. (3). However, the viscous stress tensor is needed to write the stress continuity at the interface. The viscous stress in the surrounding liquid is the classic one in the context of Rayleigh–Plesset equation; it can be re-derived here with Eq. (13) and $\dot{A} = 0$, $\dot{B} = R_2^2 \dot{R}_2$. Neglecting the surface tensions, the continuity of normal stresses at interfaces is thus written as

$$-p(R_2) - 4\mu\frac{\dot{R}_2}{R_2} = \sigma^s_{rr}(R_2), \tag{19a}$$

$$\sigma^s_{rr}(R_1) = \sigma^c_{rr}(R_1). \tag{19b}$$

The system of equation is now closed, and finally, replacing Eqs. (19) in Eq. (3) leads to a set of two coupled differential equations governing the radial motion of the compressible particle,

$$\rho\left[R_2\ddot{R}_2 + \frac{3}{2}\dot{R}_2^2 - \frac{1}{c}\left(R_2^2 \dddot{R}_2 + 6R_2\dot{R}_2\ddot{R}_2 + 2\dot{R}_2{}^3\right)\right] = p_0 - p_\infty - 4\mu\frac{\dot{R}_2}{R_2} - M^s \ln\left(\frac{R_2^3 - R_1^3}{R_{20}^3 - R_{10}^3}\right) + 4G^s \ln\left(\frac{R_2}{R_{20}}\right) - 3\zeta^s \frac{R_2^2\dot{R}_2 - R_1^2\dot{R}_1}{R_2^3 - R_1^3} + 4\mu^s \frac{R_1^3}{R_2^3 - R_1^3}\left(\frac{\dot{R}_1}{R_1} - \frac{\dot{R}_2}{R_2}\right), \tag{20a}$$

$$3K^c \ln\left(\frac{R_1}{R_{10}}\right) + 3\zeta^c \frac{\dot{R}_1}{R_1} - M^s \ln\left(\frac{R_2^3 - R_1^3}{R_{20}^3 - R_{10}^3}\right) + 4G^s \ln\left(\frac{R_1}{R_{10}}\right) - 3\zeta^s \frac{R_2^2\dot{R}_2 - R_1^2\dot{R}_1}{R_2^3 - R_1^3} + 4\mu^s \frac{R_2^3}{R_2^3 - R_1^3}\left(\frac{\dot{R}_1}{R_1} - \frac{\dot{R}_2}{R_2}\right) = 0, \tag{20b}$$

where we noted $M^s = K^s + 4/3G^s$ the longitudinal modulus in the shell material

The system of Eqs. (20) is a generalization of Church's model, taking into account shell compressibility. It is the main result of the present work. Let us recall that surface tension terms and inertial effects of the shell are neglected here. The absence of shell inertia comes from the linearization of the equation of continuity, Eq. (4). Smallness of shell inertia was justified in Ref. 12 for nano-droplets. Because we did not consider any pre-stressed equilibrium of the particle, the equilibrium radius $R_{1\mathrm{eq}}$, introduced by Church as the inner radius of the unconstrained particle,[13] does not appear in Eqs. (20).

III. INFLUENCE OF SHELL COMPRESSIBILITY

A. Linearization

The derivation of an analytical solution for the dynamics of the particle is of interest for comparing theory with measurements of speed of sound and attenuation by acoustic spectroscopy.[20] In the framework of linear ultrasound propagation, one now assumes that the oscillations due to the external pressure field are of low amplitude, so that any quantity $q(t)$ is written $q(t) = q_0 + q_a(t)$ with index 0 for static values independent of time and space, and index a for acoustical perturbations. Eqs. (20) governing the radial motion of the particle become, after linearization,

$$p_a = -\rho_0 R_{20}^2\left(\ddot{r}_{2a} - \frac{R_{20}}{c}\dddot{r}_{2a}\right) - (3K^c + 4G^s)\, r_{1a} - 3\zeta^c \dot{r}_{1a} + (4G^s) r_{2a} - 4\mu\dot{r}_{2a} - 4\mu^s(\dot{r}_{1a} - \dot{r}_{2a}), \tag{21a}$$

$$0 = (3K^c + 4G^s)\, r_{1a} + 3\zeta^c \dot{r}_{1a} - 3M^s \frac{V_{20}r_{2a} - V_{10}r_{1a}}{V_{S0}} - 3\zeta^s \frac{V_{20}\dot{r}_{2a} - V_{10}\dot{r}_{1a}}{V_{S0}} + 4\mu^s \frac{V_{20}}{V_{S0}}(\dot{r}_{1a} - \dot{r}_{2a}), \tag{21b}$$

where we have set the dimensionless variables $r_{1a}(t) = R_{1a}(t)/R_{10}$ and $r_{2a}(t) = R_{2a}(t)/R_{20}$, and where $V_{10} = 4\pi R_{10}^3/3$, $V_{20} = 4\pi R_{20}^3/3$, and $V_{S0} = V_{20} - V_{10}$ are the volumes of the core, of the particle, and of the shell at rest, respectively. In the particular case of an harmonic excitation, any component q_a of the acoustic field (p_a, r_{1a}, r_{2a}) is written $q_a = \hat{q}_a \exp[-i\omega t]$ with $\omega = 2\pi f$ the angular frequency. Equations (21) then reduce to

$$\hat{p}_a = \left[\rho_0 R_{20}^2\omega^2\left(1 + i\omega\frac{R_{20}}{c}\right) + 4\tilde{G}^s + 4i\omega\mu\right]\hat{r}_{2a} - \left(3\tilde{K}^c + 4\tilde{G}^s\right)\hat{r}_{1a}, \tag{22a}$$

$$0 = \left(3\tilde{K}^c + 4\tilde{G}^s\right)\hat{r}_{1a} - 3\tilde{M}^s \frac{V_{20}\hat{r}_{2a} - V_{10}\hat{r}_{1a}}{V_{S0}}. \tag{22b}$$

Here we have introduced the complex dynamical moduli

$$\tilde{K}^s = K^s - i\omega\zeta^s, \tag{23a}$$

$$\tilde{G}^s = G^s - i\omega\mu^s, \tag{23b}$$

$$\tilde{K}^c = K^c - i\omega\zeta^c, \tag{23c}$$

which take into account the viscoelastic behavior of the shell and of the core, and where $\tilde{M}^s = \tilde{K}^s + 4\tilde{G}^s/3$.

Equation (22b) gives the relation between the inner and outer radius and can be written equivalently

$$\frac{\hat{r}_{2a}}{\hat{r}_{1a}}\frac{V_{20}}{V_{10}} = 1 + \frac{V_{S0}}{V_{10}}\frac{\tilde{K}^c + \frac{4}{3}\tilde{G}^s}{\tilde{M}^s} \equiv 1 + \chi. \tag{24}$$

In the case of an incompressible shell,[13] this equation is replaced by the condition of incompressibility $R_1^2\dot{R}_1 = R_2^2\dot{R}_2$. One can notably point out that in the linear harmonic regime, this condition reduces to $\hat{r}_{2a}/\hat{r}_{1a} = V_{10}/V_{20}$, so Eq. (24) reduces to $\chi = 0$. The hypothesis of incompressibility is thus valid in two cases. The first one is the case of a thin shell ($V_{S0} \ll V_{10}$), assuming the ratio of material properties $(\tilde{K}^c + 4\tilde{G}^s/3)/\tilde{M}^s$ is of order 1. In particular one can note that for a particle entirely filled by the shell material and without core ($V_{10} = 0$), the incompressible assumption breaks down, leading to a mathematical singularity. The second one is the case of a soft shell material ($\tilde{G}^s \ll \tilde{K}^s$) with a core much more compressible than the shell ($\tilde{K}^c \ll \tilde{K}^s$). Finally, reporting Eq. (24) in Eq. (22a) allows one to derive the relation between the acoustic pressure and the outer radius $\hat{p}_a = C(\omega)\hat{R}_{2a}$ with

$$C(\omega) = \omega^2\rho_0 R_{20}\left(1 + i\omega\frac{R_{20}}{c}\right) - 3\frac{\tilde{K}^c}{R_{20}}\frac{(1+\eta)^3}{1+\chi} - 4\frac{\tilde{G}^s}{R_{20}}\left(\frac{(1+\eta)^3}{1+\chi} - 1\right) + 4i\frac{\omega}{R_{20}}\mu, \tag{25}$$

where $\eta = h_0/R_{10}$ is the ratio of the shell thickness $h_0 = R_{20} - R_{10}$ to the inner radius. One can note that for an incompressible shell, thus setting $\chi = 0$, this solution is equivalent to that given by Eq. (19) in Ref. 12 when one neglects surface tensions and inertia of the shell.

B. Quantification of compressibility effects

As the effect of the shell compressibility is entirely included in the function $\chi(\omega)$, its study may be of particular interest at this point. One can notably observe that the quantity

$$\frac{V_{10}}{V_{S0}}\chi = \frac{\tilde{K}^c + \frac{4}{3}\tilde{G}^s}{\tilde{M}^s} \tag{26}$$

behaves similarly to a Zener type rheological model,

$$\frac{V_{10}}{V_{S0}}\chi = \beta_0 - i\omega\tau_{ch}\frac{\beta_\infty}{1 - i\omega\tau_{ch}}, \tag{27}$$

defined by the characteristic time

$$\tau_{ch} = \frac{1}{2\pi f_{ch}} = \frac{\zeta^s + \frac{4}{3}\mu^s}{K^s + \frac{4}{3}G^s}, \tag{28}$$

the low frequency ratio of elastic moduli,

$$\beta_0 = \frac{K^c + \frac{4}{3}G^s}{K^s + \frac{4}{3}G^s}, \tag{29}$$

and the high frequency ratio of viscous moduli,

$$\beta_0 + \beta_\infty = \frac{1 + \frac{3}{4}\frac{\zeta^c}{\mu^s}}{1 + \frac{3}{4}\frac{\zeta^s}{\mu^s}}. \tag{30}$$

In order to illustrate this point, we consider a particle close to nanometric medical contrast agents, and we simplify the analysis by setting $V_{S0} = V_{10}$ ($h_0/R_{20} \simeq 0.2$). The core is liquid perfluorooctyl bromide (PFOB) characterized[21] by its density $\rho^c = 1918\,\mathrm{kg\,m^{-3}}$ and speed of sound $c^c = 624\,\mathrm{m\,s^{-1}}$, so that $K^c \simeq 0.75$ GPa; the bulk viscosity of PFOB is $\zeta^c = 5 \times 10^{-3}$ Pa s. The shell parameters are chosen in the range of those of typical biocompatible polymers such as poly(lactid-*co*-glycolid) acid (PLGA):[12] $G^s = 1$ GPa, $K^s = 6.4$ GPa, $\mu^s = 1$ Pa s, which give a speed of sound for longitudinal waves $V_L \simeq 2400\,\mathrm{m\,s^{-1}}$, in agreement with measurements.[22]

Figure 2 presents the quantity χ as function of the frequency, and for three values of the bulk viscosity ζ^s of the shell around the critical value $\zeta^s_{crit} \simeq 4$ Pa s. The latter corresponds to the particular case for which the effect of shell compressibility becomes independent of frequency ($\beta_\infty = 0$), i.e., when the viscous and elastic properties verify the relation

$$\zeta^s_{crit} = \frac{\zeta^c\left[K^s + \frac{4}{3}G^s\right] + \frac{4}{3}\mu^s[K^s - K^c]}{K^c + \frac{4}{3}G^s}. \tag{31}$$

One can clearly observe that the shell compressibility introduces an apparent "relaxing" behavior, even though no

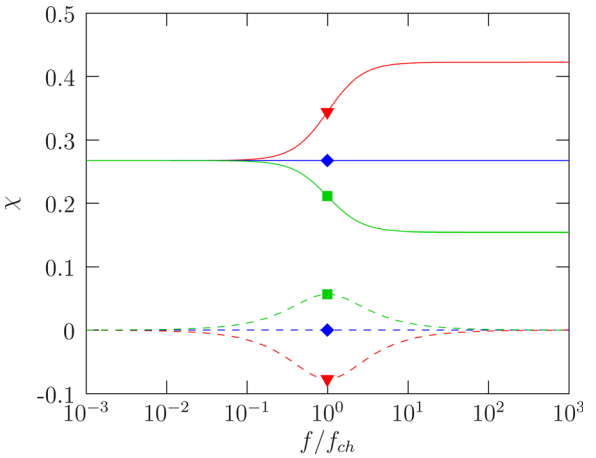

FIG. 2. (Color online) Real (—) and imaginary (−−) parts of the function $\chi(\omega)$ for three values of the bulk viscosity ζ^s: $\zeta^s/\zeta^s_{crit} = 0.5$ (▼), $\zeta^s/\zeta^s_{crit} = 1$ (◆), and $\zeta^s/\zeta^s_{crit} = 2$ (■), where ζ^s_{crit} is the critical value defined by Eq. (31). The frequency is normalized with the characteristic frequency of the compressible shell.

relaxation model has been considered for the rheology of the shell. As discussed previously, the function χ is the product of the shell to core volumes ratio V_{S0}/V_{10} with a frequency-dependent complex quantity comparable with a relaxing Zener modulus. This means that in low- and high-frequency asymptotic cases – relative to the characteristic frequency $f_{ch} = 1/(2\pi\tau_{ch})$, χ is purely real. Obviously, for these two limiting cases, χ does not necessarily converge towards 0, but towards a finite value which depends on the shell thickness and on the viscoelastic properties. Because we restrained our study to the case of a viscoelastic Kelvin–Voigt model for the shell, the low-frequency behavior of χ is governed by the elastic properties of the particles, while the viscous ones govern the high-frequency limit case. For example, in Fig. 2, as χ is obtained for different values of the bulk viscosity ζ^s of the shell, its real part is only affected for high frequencies. Around the characteristic frequency, both elasticity and viscosity affect the function χ, notably the imaginary part which reaches an extremum. The curves denoted by a diamond (◆) represent the particular case $\zeta^s = \zeta^s_{crit}$ for which low- and high-frequency limit values are the same, and a relaxation effect is not observed anymore. If $\zeta^s > \zeta^s_{crit}$ (■), the shell will be closer to the incompressible case above rather than below the characteristic frequency. If $\zeta^s < \zeta^s_{crit}$ (▼), the opposite behavior is obtained and the effect of compressible shell will be stronger above f_{ch}.

The results illustrated by Fig. 2 show that taking into account the compressibility introduces an apparent relaxing behavior of the shell. As PLGA is known to be a glassy polymer,[23] it hence becomes naturally interesting to study how a relaxing rheological model for the viscoelastic shell can affect the dynamics of the particle. Because the equations are derived in the linear harmonic approximation, introducing a rheological behavior of the Zener type for the shell is quite straightforward and simply consists in replacing the dynamical moduli Eq. (23a) and Eq. (23b) by the following expressions:[24]

$$\tilde{K}^s = K^s - i\omega\tau^s \frac{K^s_\infty}{1 - i\omega\tau^s}, \tag{32a}$$

$$\tilde{G}^s = G^s - i\omega\tau^s \frac{G^s_\infty}{1 - i\omega\tau^s}, \tag{32b}$$

where τ^s is the relaxation time of the shell material. Replacing Eqs. (32) into Eq. (26) then leads to a new form of Eq. (27) which becomes

$$\frac{V_{10}}{V_{S0}}\chi = \beta_0 - i\omega\tau'_{ch}\frac{\beta'_\infty}{1 - i\omega\tau'_{ch}} - \omega^2 \frac{\zeta^c}{1 - i\omega\tau'_{ch}}\left(\frac{\tau^s}{K^s + \frac{4}{3}G^s}\right), \tag{33}$$

with $\tau'_{ch} = \tau_{ch} + \tau^s$ and $\beta'_\infty = [\tau_{ch}/(\tau_{ch} + \tau^s)]\beta_\infty$. This new expression for χ is plotted in Fig. 3 for two values of the relaxation time τ^s. The last term in Eq. (33) is due to the viscosity of the core and has an effect essentially on the imaginary part of χ at high frequencies; this term vanishes if we neglect the bulk viscosity of the core. This latter put aside, Eq. (33) has the same form as Eq. (27). Moreover, the low-frequency elastic term β_0 is not modified. However, taking into account relaxation for the shell material reduces the characteristic frequency and the high-frequency asymptotic value of χ. On the one hand, when the relaxation frequency of the shell material is very large ($\tau^s \ll \tau_{ch}$), then $\beta'_\infty \to \beta_\infty$ and $\tau'_{ch} \to \tau_{ch}$ and one recovers Eq. (27) obtained for the Kelvin–Voigt model. On the other hand, when the relaxation frequency of the shell material is sufficiently low ($\tau^s \gg \tau_{ch}$), then $\beta'_\infty \to 0$ and $\tau'_{ch} \to \tau^s$, so that the shell rheology overcomes the apparent relaxation of the compressible shell.

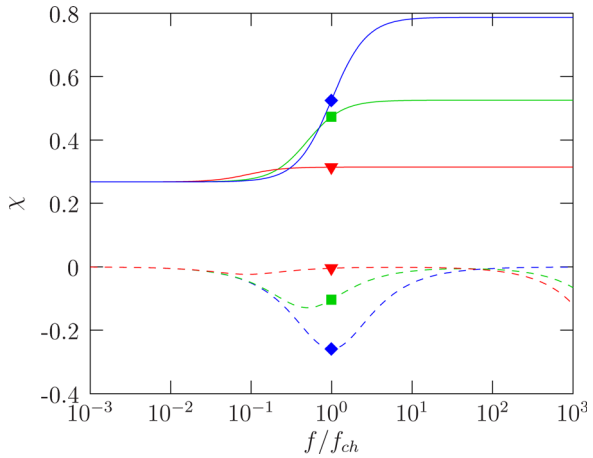

FIG. 3. (Color online) Effect of a rheological Zener model on the real (—) and imaginary (- -) parts of the function $\chi(\omega)$. The frequency is normalized with the characteristic frequency f_{ch}. The results obtained for a Kelvin–Voigt model are represented by ◆. The symbols ■ and ▼ are for the Zener model, with $\tau^s = \tau_{ch}$ and $\tau^s = 10\tau_{ch}$, respectively.

IV. BALANCE EQUATIONS FOR POLYDISPERSE SOLUTIONS

The equations derived in the previous section are those of the generalized Church's model for a droplet encapsulated by a compressible shell. When replaced into the model described in Ref. 12, these equations—and especially Eq. (25)—describe the propagation of a harmonic plane wave in a monodisperse solution of particles. In the present section, this model is reformulated in order to take into account the polydispersity both in particle size and shell thickness. The suspension is constituted of two phases, namely, the particles whose dynamics have been derived beforehand, and the ambient fluid. The average fluid phase field satisfies the balance equations of mass and momentum,

$$\frac{\partial}{\partial t}[(1 - \Phi)\rho] + \nabla \cdot [(1 - \Phi)\rho\mathbf{v}] = 0, \tag{34a}$$

$$(1 - \Phi)\rho\left[\frac{\partial \mathbf{v}}{\partial t} + (\mathbf{v} \cdot \nabla)\mathbf{v}\right] - \nabla \cdot \sigma^l = -\mathbf{f}, \tag{34b}$$

where the specific mass of the fluid is weighted by the fluid volume fraction $1 - \Phi$. Here $\Phi(\mathbf{x}, t)$ denotes the local volume fraction of particles and $-\mathbf{f}(\mathbf{x}, t)$ is the total force per unit volume exerted by all particles onto the fluid phase. The stress tensor σ^l in the liquid is

$$\sigma^l = \left[-p + \left(\zeta - \frac{2}{3}\mu\right)\nabla\cdot\mathbf{v}\right]\mathbf{I} + 2\mu\mathbf{D}, \tag{35}$$

with $\mathbf{I}$ the unit tensor and $\mathbf{D}$ the rate-of-strain tensor. Bulk (ζ) and shear (μ) viscosities may be modified by the presence of particles but, in the dilute case, they are almost identical to those of the pure fluid phase.

A nanodroplet at position $\mathbf{x}$ and time t is characterized by its inner radius $R_1(\mathbf{x}, t)$ and outer radius $R_2(\mathbf{x}, t)$, whose dynamics have been described in the previous section. We assume that, in the static case with no acoustic field, droplets have a distribution in both size and thickness. We note by $\mathbf{a} = (R_{10}, R_{20})$ the two values of the inner and outer static radii for a given droplet, and by $n(\mathbf{a}, \mathbf{x}, t)$ the number of particles per unit volume at point $\mathbf{x}$ and time t, whose static geometrical parameters are within the range $\mathbf{a} = (R_{10}, R_{20})$ and $\mathbf{a} + d\mathbf{a} = (R_{10} + dR_{10}, R_{20} + dR_{20})$. The suspension is assumed to be homogeneous, so that the static distribution function $n_0(\mathbf{a})$ is independent of space. The total volume of a droplet is $V_2(\mathbf{a}, \mathbf{x}, t) = \frac{4}{3}\pi R_2^3$, its outer surface $S_2(\mathbf{a}, \mathbf{x}, t) = 4\pi R_2^2$, and its mass is $m_P(\mathbf{a}) = \frac{4}{3}\pi\left[\rho^c R_1^3 + \rho^s(R_2^3 - R_1^3)\right]$. Each droplet is assumed to be impermeable, hence $m_P(\mathbf{a})$ is independent on time and space. Droplet density is $\rho_P(\mathbf{a}, \mathbf{x}, t) = m_P(\mathbf{a})/V_2(\mathbf{a}, \mathbf{x}, t)$, where $V_2(\mathbf{a}, \mathbf{x}, t)$ is the volume of the particle. The volume fraction of particles is

$$\Phi(\mathbf{x}, t) = \int\int n(\mathbf{a}, \mathbf{x}, t) V_2(\mathbf{a}, \mathbf{x}, t) d\mathbf{a}. \tag{36}$$

The number of particles characterized by parameters $\mathbf{a}$ is constant, hence there is no droplet fragmentation or coalescence,

$$\frac{\partial n(\mathbf{a}, \mathbf{x}, t)}{\partial t} + \nabla.[n(\mathbf{a}, \mathbf{x}, t)\mathbf{v}_P(\mathbf{a}, \mathbf{x}, t)] = 0, \tag{37}$$

so that the number $n(\mathbf{a}, \mathbf{x}, t)$ of particles characterized by parameters $\mathbf{a}$ per unit volume evolves only because of the flow of particles in and out of the considered volume at the particle velocity $\mathbf{v}_P(\mathbf{a}, \mathbf{x}, t)$. We denote by $\mathbf{F}(\mathbf{a}, \mathbf{x}, t)$ the force exerted by the fluid onto a single particle characterized by geometrical parameters $\mathbf{a}$:

$$m_P(\mathbf{a})\left[\frac{\partial}{\partial t} + (\mathbf{v}_P(\mathbf{a}, \mathbf{x}, t).\nabla)\right]\mathbf{v}_P(\mathbf{a}, \mathbf{x}, t) = \mathbf{F}(\mathbf{a}, \mathbf{x}, t). \tag{38}$$

The total force per unit volume exerted by the fluid onto the ensemble of particles is therefore

$$\mathbf{f}(\mathbf{x}, t) = \int\int n(\mathbf{a})\mathbf{F}(\mathbf{a}, \mathbf{x}, t) d\mathbf{a}. \tag{39}$$

In the linear acoustic approximation, any quantity $q(\mathbf{a}, \mathbf{x}, t)$ is written $q(\mathbf{a}, \mathbf{x}, t) = q_0(\mathbf{a}) + q_a(\mathbf{a}, \mathbf{x}, t)$. At static equilibrium, the medium is homogeneous and $q_0(\mathbf{a})$ is independent on space. There is also no ambient flow motion so that $\mathbf{v}_0 = \mathbf{v}_{P0} = 0$ (in order to simplify the notations, $\mathbf{v}$ and $\mathbf{v}_P$ will denote the acoustic velocities in the fluid and droplet phases). After linearization, mass and momentum balance equations (34) get

$$(1 - \Phi_0)\left(\frac{\partial \rho_a}{\partial t} + \rho_0 \nabla.\mathbf{v}\right) = \rho_0 \frac{\partial \Phi_a}{\partial t}, \tag{40a}$$

$$(1 - \Phi_0)\rho_0 \frac{\partial \mathbf{v}}{\partial t} + \nabla p_a = \left(\zeta - \frac{2}{3}\mu\right)\nabla(\nabla.\mathbf{v}) + 2\mu\nabla\cdot\mathbf{D}_a - \int\int n_0(\mathbf{a})\mathbf{F} d\mathbf{a}. \tag{40b}$$

Linearization of Eqs. (36)–(38) yields

$$\frac{\partial \Phi_a}{\partial t} = \int\int\left[\frac{\partial n_a(\mathbf{a})}{\partial t} V_{20}(\mathbf{a}) + n_0(\mathbf{a}) 4\pi R_{20}^2 \frac{\partial R_{2a}}{\partial t}\right] d\mathbf{a}, \tag{41a}$$

$$\frac{\partial n(\mathbf{a})}{\partial t} = -n_0(\mathbf{a})\nabla\cdot\mathbf{v}_P(\mathbf{a}), \tag{41b}$$

$$m_P(\mathbf{a})\frac{\partial \mathbf{v}_P}{\partial t} = \mathbf{F}. \tag{41c}$$

For a compressible fluid in adiabatic evolution, the state equation can be linearized as $p_a = c^2\rho_a$: this amounts to neglect thermal effects on sound propagation in the fluid, which are proportional to $\gamma - 1$, where γ is the ratio of specific heats at constant pressure and volume. For water, this ratio is extremely close to one, hence that approximation is well satisfied. Eliminating variables ρ_a, n_a, and Φ_a one obtains the following system of seven equations and seven unknowns (p_a, $\mathbf{v}$, $\mathbf{v}_P$), where the mass balance equation for the fluid phase Eq. (40a) is

$$(1 - \Phi_0)\left(\frac{\partial p_a}{\partial t} + \rho_0 c^2 \nabla\cdot\mathbf{v}\right) = \rho_0 c^2 \int\int n_0(\mathbf{a})\left[4\pi R_{20}^2 \frac{\partial R_{2a}}{\partial t} - V_{20}(\mathbf{a})\nabla\cdot\mathbf{v}_P(\mathbf{a})\right] d\mathbf{a}. \tag{42}$$

It is complemented by the momentum equations for the fluid and droplet [Eqs. (40b)–(41c)] phases. For a monodisperse suspension with particles of single radii $\mathbf{a}_0 = (\langle R_{10}\rangle, \langle R_{20}\rangle)$, one has $n_0(\mathbf{a}) = n_0\delta(\mathbf{a} - \mathbf{a}_0)$ with δ the two-dimensional Dirac distribution. Then one recovers Eqs. (8)–(10) of Ref. 12.

The force exerted by the fluid phase on a single particle in the linear regime is given by the Faxén formula[14,15]

$$\mathbf{F} = 6\pi R_{20}\mu(\mathbf{v} - \mathbf{v_P}) + 6R_{20}^2\sqrt{\pi\rho_0\mu}\int_{-\infty}^{t}\frac{\partial}{\partial t'}(\mathbf{v} - \mathbf{v_P})\frac{dt'}{\sqrt{t - t'}} + \frac{2}{3}\pi R_{20}^3\rho_0\frac{\partial}{\partial t}(\mathbf{v} - \mathbf{v_P}) + \frac{4}{3}\pi R_{20}^3\rho_0\frac{\partial \mathbf{v}}{\partial t}, \tag{43}$$

which is independent on the droplet shell thickness R_{10}.

V. DISPERSION RELATION

The dispersion relation for an acoustic wave propagating in such a medium can now be computed. Longitudinal waves are considered, for which the velocity and force fields

$(\mathbf{v}, \mathbf{v}_P, \mathbf{F}) = (v, v_P, F)\mathbf{x}$ are parallel to the direction $\mathbf{x}$ of wave propagation. Any component q_a of the acoustic field $(p_a, v, v_P, R_{1a}, R_{2a}, F)$ is written $q_a = \hat{q}_a \exp[i(kx - \omega t)]$ with k the wavenumber.

The Fourier transform of Eq. (43) yields

$$\hat{F}(\mathbf{a}, \mathbf{x}, \omega) = F_A(\mathbf{a}, \omega)\hat{v}(\mathbf{x}, \omega) + F_B(\mathbf{a}, \omega)[\hat{v}(\mathbf{x}, \omega) - \hat{v}_P(\mathbf{a}, \mathbf{x}, \omega)], \quad (44a)$$

$$F_A(\mathbf{a}, \omega) = -\frac{4}{3}\pi R_{20}^3 \rho_0 i\omega, \quad (44b)$$

$$F_B(\mathbf{a}, \omega) = 6\pi R_{20}\mu + 3\pi\sqrt{2\rho_0\mu\omega}R_{20}^2(1 - i) - \frac{2}{3}\pi R_{20}^3\rho_0 i\omega. \quad (44c)$$

By noting that $F_A(\mathbf{a}, \omega) = -i\omega m_P(\mathbf{a})/r_P(\mathbf{a})$, where $r_P(\mathbf{a}) = \rho_{P0}(\mathbf{a})/\rho_0$, Eq. (41c) for particle motion simplifies into

$$\hat{v}_P(\mathbf{a}, \mathbf{x}, \omega) = \frac{F_A(\mathbf{a}, \omega) + F_B(\mathbf{a}, \omega)}{F_B(\mathbf{a}, \omega) + r_P(\mathbf{a})F_A(\mathbf{a}, \omega)}\hat{v}(\mathbf{a}, \mathbf{x}, \omega) = W(\mathbf{a}, \omega)\hat{v}(\mathbf{a}, \mathbf{x}, \omega), \quad (45)$$

so that

$$\hat{F}(\mathbf{a}, \omega) = -i\omega m_P(\mathbf{a})W(\mathbf{a}, \omega)\hat{v}(\mathbf{x}, \omega). \quad (46)$$

The momentum balance equation Eq. (40b) reduces to

$$k\hat{p}_a = \left[\omega[(1 - \Phi_0)\rho_0 + \rho_A(\omega)] + \left(\frac{4}{3}\mu + \zeta\right)ik^2\right]\hat{v}. \quad (47)$$

Here,

$$\rho_A(\omega) = \int\int n_0(\mathbf{a})m_P(\mathbf{a})W(\mathbf{a}, \omega)d\mathbf{a} \quad (48)$$

is an apparent complex and frequency-dependent density associated to the droplets motion relative to the ambient fluid that adds to the ambient fluid density and modifies the impedance relation (47) between the pressure and velocity fields. The mass balance Eq. (42) reduces to

$$\left[(1 - \Phi_0) - \rho_0 c^2 \int\int n_0(\mathbf{a})S_{20}(\mathbf{a})C^{-1}(\mathbf{a}, \omega)d\mathbf{a}\right]\hat{p}_a = \rho_0 c^2 \frac{k}{\omega}\left[(1 - \Phi_0) + \int\int n_0(\mathbf{a})V_{20}(\mathbf{a})W(\mathbf{a}, \omega)d\mathbf{a}\right]\hat{v}, \quad (49)$$

where C is given by Eq. (25). Combining Eqs. (47) and (49) finally leads to the dispersion relation

$$\left(\frac{k}{k^*}\right)^2 = \left(\frac{1 - \Phi_0}{1 - i\omega\tau_V\frac{1 - D}{1 + T}}\right)(1 - D)\left(\frac{1 + rT}{1 + T}\right), \quad (50)$$

with $k^* = \omega/c$ the wave number in the ambient fluid with no particle, and

$$\tau_V = \frac{1}{\rho_0 c^2}\left(\zeta + \frac{4}{3}\mu\right), \quad (51a)$$

$$T(\omega) = \frac{1}{1 - \Phi_0}\int\int n_0(\mathbf{a})V_{20}(\mathbf{a})W(\mathbf{a}, \omega)d\mathbf{a}, \quad (51b)$$

$$r(\omega) = \frac{\rho_A(\omega)}{(1 - \Phi_0)\rho_0 T(\omega)}, \quad (51c)$$

$$D(\omega) = \frac{\rho_0 c^2}{1 - \Phi_0}\int\int \frac{n_0(\mathbf{a})S_{20}(\mathbf{a})}{C(\mathbf{a}, \omega)}d\mathbf{a}. \quad (51d)$$

In Eq. (50), τ_V is the characteristic time measuring bulk absorption of sound in the ambient fluid. Translational effects due to the visco-inertial Faxén forces exerted on the particles (considered as almost rigid) are described by coefficients T and r. Dilatational effects due to the change of particle volume are described by coefficient D. As expected, in the dilute approximation, all three terms are proportional to the particle volume fraction $\Phi_0 = n_0 V_0$. In the case of pure ambient fluid ($\Phi_0 = T = D = 0$), and in the considered frequency range where $\omega\tau_V \ll 1$, one recovers the usual dispersion relation in a viscous fluid $k = k^* + i\omega^2\tau_V/2c$.

Equation (50) is valid in general for any dilute suspension of polydispersed liquid droplets or gaseous bubbles encapsulated with a viscoelastic shell. It combines simultaneously the translational motion of the particles induced by visco-inertial coupling with the ambient fluid (described by the T and r terms), and the dilatational deformation of the particles due to the shell visco-elasticity and to core compressibility (described by the D term). It recovers the Church's model[13] for encapsulated contrast agents, Commander and Prosperetti's model[25] for bubbly liquids (with thermal effects neglected). Through the translational part, it also recovers previous models for rigid[26] and deformable[12] particles.

VI. RESULTS

In order to validate the model for ultrasonic agents potentially used for medical drug delivery, the simulations are performed for a suspension of liquid PFOB droplets encapsulated by a shell of biocompatible polymer, with a volume fraction of 1%. At rest, one particle is characterized by its outer radius $R_{20} = 100\,\text{nm}$. The shell thickness to outer radius ratio $h_0/R_{20} = 0.25$ is around measured typical values.[9] The ambient fluid is pure water. Some parameters of the shell are fixed equal to those used in a previous study,[12] namely, its specific mass $\rho^s = 1350\,\text{kg m}^{-3}$ and shear viscosity $\mu^s = 1\,\text{Pa s}$.

A. Effect of the shell compressibility

In Figs. 4 and 5, the phase velocity $c_\phi = \omega/\Re(k)$ and the absorption coefficient $\alpha = \Im(k)$—where $\Re(\cdots)$ and $\Im(\cdots)$ denote the real and imaginary parts of a complex number, respectively—are calculated for several values of the viscoelastic parameters of the shell. The frequency range is limited to [1–100] MHz, including medical range.

In Fig. 4, computations are made for a quite low shear modulus $G^s = 300\,\text{MPa}$ relative to bulk modulus $K^s = 7.4\,\text{GPa}$, thus corresponding to a critical value $\zeta^s_{\text{crit}} = 7.7\,\text{Pa s}$, according to Eq. (31), and to a Poisson ratio $\nu = 0.48$ (close to the

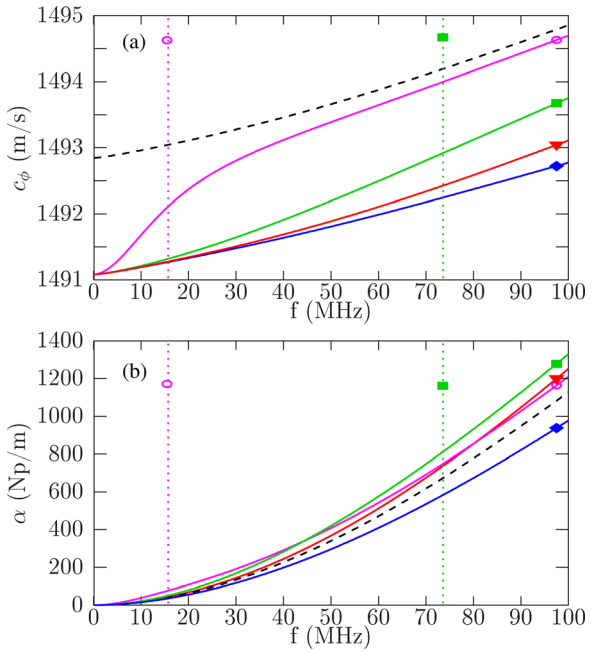

FIG. 4. (Color online) Sound velocity (a) and absorption coefficient (b) for $G^s = 300$ MPa, $K^s = 7.4$ GPa, and for four values of the bulk viscosity ζ^s. ◆: $\zeta^s/\zeta^s_{\text{crit}} = 0.1$; ▼: $\zeta^s/\zeta^s_{\text{crit}} = 1$; ■: $\zeta^s/\zeta^s_{\text{crit}} = 2$; ○: $\zeta^s/\zeta^s_{\text{crit}} = 10$, with $\zeta^s_{\text{crit}} = 7.7$ Pa s. Dashed line: incompressible shell. The vertical dotted lines mark the location of the characteristic frequency f_{ch} for each case with the same symbol code.

incompressible limit $\nu = 0.5$). The results corresponding to ratios $\zeta^s/\zeta^s_{\text{crit}} = 0.1$ (◆), $\zeta^s/\zeta^s_{\text{crit}} = 1$ (▼), $\zeta^s/\zeta^s_{\text{crit}} = 2$ (■), and $\zeta^s/\zeta^s_{\text{crit}} = 10$ (○) are compared with those obtained for an incompressible shell (dashed lines), thus setting $\chi = 0$ in Eq. (25). Independently of the frequency, taking into account

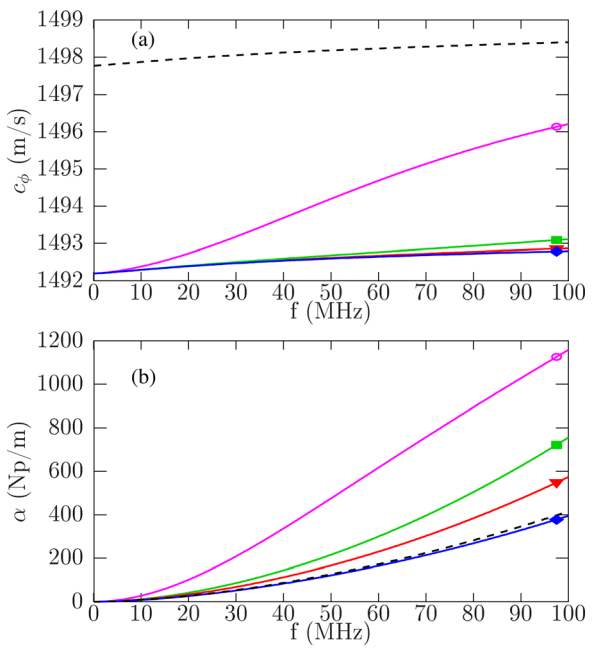

FIG. 5. (Color online) Sound velocity (a) and absorption coefficient (b) for $G^s = 3$ GPa, $K^s = 3.8$ GPa, and for four values of the bulk viscosity ζ^s. ◆: $\zeta^s/\zeta^s_{\text{crit}} = 0.1$; ▼: $\zeta^s/\zeta^s_{\text{crit}} = 1$; ■: $\zeta^s/\zeta^s_{\text{crit}} = 2$; ○: $\zeta^s/\zeta^s_{\text{crit}} = 10$, with $\zeta^s_{\text{crit}} = 0.86$ Pa s. Dashed line: incompressible shell. The vertical dotted lines mark the location of the characteristic frequency f_{ch} for each case with the same symbol code.

the compressibility of the shell leads to a lower phase velocity than in the incompressible case since the particle becomes less rigid. The elastic properties being the same for the four cases, the low-frequency values for speed of sound c_ϕ and absorption α thus converge towards the same limits for the four curves. When the bulk viscosity is fixed to 10 times the critical value (○), the dispersion curve for the compressible shell shows a large difference with the incompressible case (black dashed line) below the characteristic frequency but converge towards it for highest frequencies: we are typically in the same conditions as the ■ curve presented in Fig. 2. Moreover, decreasing the bulk viscosity leads to a rise of the transition frequency. The results obtained for $\zeta^s/\zeta^s_{\text{crit}} = 0.1$ and $\zeta^s/\zeta^s_{\text{crit}} = 1$ are of particular interest because the characteristic frequency becomes so high that it is not visible on the frequency range. For both cases, the whole shift of the dispersion curve relative to the incompressible shell case is essentially due to the elasticity of the shell and a relaxation behavior is not observable anymore. It is also important to point out that for the first case, since $\zeta^s/\zeta^s_{\text{crit}} < 1$, the function χ is characterized by a negative imaginary part (see the ▼ curve presented in Fig. 2), which explains why the absorption is lower for the compressible shell than for the incompressible case. On the other hand for the three other cases, the absorption is higher for the compressible shell as $\zeta^s/\zeta^s_{\text{crit}} \geq 1$ and the dispersion curves become closer to the incompressible shell as the bulk viscosity becomes larger.

The results given in Fig. 5 are similar to those in Fig. 4, but with $G^s = 3$ GPa and $K^s = 3.8$ GPa ($\zeta^s_{\text{crit}} = 0.86$ Pa s, $\nu = 0.18$), always keeping the longitudinal waves celerity $V_L = 2400\ \text{m s}^{-1}$ constant, in agreement with measured data for PLGA.[22] Increasing the shear modulus while reducing the bulk modulus has mainly two effects. First, it enlarges as expected the effect of shell compressibility. On the dispersion curves, it results into a larger difference between the compressible and incompressible cases, reaching almost $6\ \text{m s}^{-1}$ at low frequencies. One can also observe that when the K^s/G^s ratio decreases, the absorption coefficient gets more sensitive to the value of the shell bulk viscosity. Second, a larger shear modulus leads to an increase of the characteristic frequency, resulting into a sound velocity which is much less dispersive on our frequency range.

The effect of the shell thickness on the dispersion and absorption is presented in Fig. 6 for incompressible (dashed lines) and compressible (continuous lines) shells. The outer radius of the particle remaining constant and fixed at 100 nm, the results are presented for three values of the ratio h_0/R_{20}: 0.1 (▼), 0.25 (◆), and 0.4 (■), respectively. The elastic parameters are $G^s = 1$ GPa and $K^s = 6.4$ GPa ($\zeta^s_{\text{crit}} = 3.7$ Pa s, $\nu = 0.43$) and the bulk viscosity is fixed to $\zeta^s/\zeta^s_{\text{crit}} = 10$. As expected, the higher the shell relative thickness is, the more important is the role of the shell compressibility. Because of the quite small value of the transition frequency here, this effect is essentially observed for the low frequencies.

B. Effect of the polydispersity

In order to study the effect of the polydispersity, the outer radius R_{20} and the ratio of shell thickness over inner

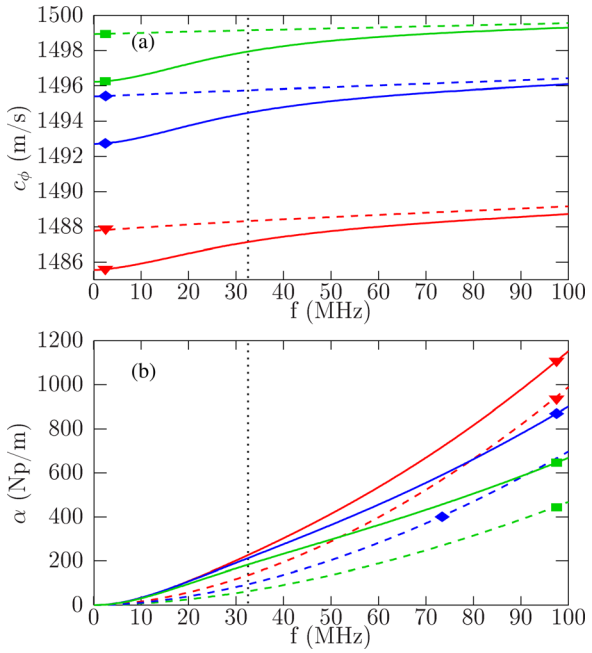

FIG. 6. (Color online) Sound velocity (a) and absorption coefficient (b) for three values of the shell thickness. ▼: $h_0/R_{20} = 0.1$; ◆: $h_0/R_{20} = 0.25$; ■: $h_0/R_{20} = 0.4$. Solid/dashed lines: compressible/incompressible shell. The vertical dotted line marks the location of the characteristic frequency f_{ch}.

radius $\eta_0 = h_0/R_{10}$ are supposed to be statistically distributed following log-normal laws around the mean values given in Table I. Modes, median values and standard deviations are also provided in this table. The speed of sound within the polydisperse solution is presented as a continuous line in Fig. 7. It is compared with the case of a monodisperse solution (dashed line) calculated from the median values $R_{20} = 138$ nm and $\eta_0 = 0.46$ of the log-normal distributions. These results show that the polydispersity has a very weak effect on the speed of sound on the whole frequency range, the largest difference being not more than $0.5\,\mathrm{m\,s^{-1}}$. We have to point out that the effect on absorption is even weaker and the difference between monodisperse and polydisperse solutions is so small that absorption curves are not presented here. Some results for polydispersity on the outer radius only ($\eta_0 = 0.46$) and polydispersity on the shell thickness only ($R_{20} = 138$ nm) are also provided in Fig. 7 (dotted lines with symbols). The change in the dispersion of the sound waves seems to be mainly due to the polydispersity on the outer radius of the particle, the polydispersity on the shell thickness being only responsible for a global decrease of the speed of sound. It is also interesting to observe that at very low

TABLE I. Statistical parameters of the log-normal distribution laws for the outer radius R_{20} and the ratio of shell thickness over inner radius $\eta_0 = h_0/R_{10}$.

	radius	thickness
mode	100 nm	1/3
median	138 nm	0.46
mean	162 nm	0.54
std. deviation	100 nm	1/3

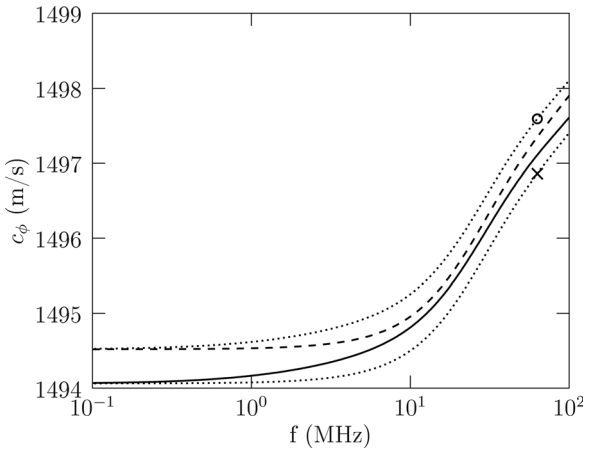

FIG. 7. Effect of the polydispersity on the sound velocity. Continuous line: double polydispersity on the outer radius R_{20} and on the ratio $\eta_0 = h_0/R_{10}$. Dashed line: case of a monodisperse solution calculated from median values of the log-normal distributions. ○: polydispersity on the outer radius only; ×: polydispersity on the ratio η_0 only.

frequencies, the polydispersity on the outer radius has no effect and one recovers the monodisperse case. On the contrary, the polydispersity on the shell thickness leads to an asymptotic value for the speed of sound which is lower than in the monodisperse case, due to the associated dispersion of particles masses.

C. Micrometric gas-filled particles

The results presented in Figs. 4–6 emphasize the role of the shell compressibility in solutions of encapsulated liquid nanodroplets. Indeed, for such objects, the compressibility and the volume of the shell are of the same order of magnitude as those of the core. It is, however, of interest to investigate larger encapsulated gaseous bubbles similar to standard contrast agents in order to quantify the validity of the incompressible hypothesis.

In this section, we consider a 1%-diluted solution of micrometric air bubbles of outer radius $R_{20} = 10$ μm and encapsulated by a thin shell of thickness $h_0 = R_{20} - R_{20} = 15$ nm, similar to those investigated by Church in his paper.[13] The values of the shell material are $\rho^s = 1100\,\mathrm{kg\,m^{-3}}$; $\mu^s = 5 \times 10^{-2}$ Pa s; $G^s = 15$, 88.8, and 150 MPa; and the bulk modulus is fixed to $K^s = 1$ GPa. The bulk viscosity ζ^s is taken equal to the critical value defined by Eq. (31), therefore depending on the value of G^s.

Figure 8 gives the sound velocity and absorption coefficient on the frequency range [1–100] MHz for the three values of the shear modulus G^s given above. Compared with the solutions of nanometric particles, larger particles become resonant.[25] One can notably observe that the compressible behavior of the shell slightly decrease the resonance frequency. Moreover, Fig. 8 shows that for large bubbles and small values of G^s, the curves become practically superimposed, thus recovering Church's model.[13] This means that, while the compressibility of the shell is of importance for droplets of nanometric size, its effect remains very weak for larger gaseous particles. The incompressibility assumption is thus valid in this case.

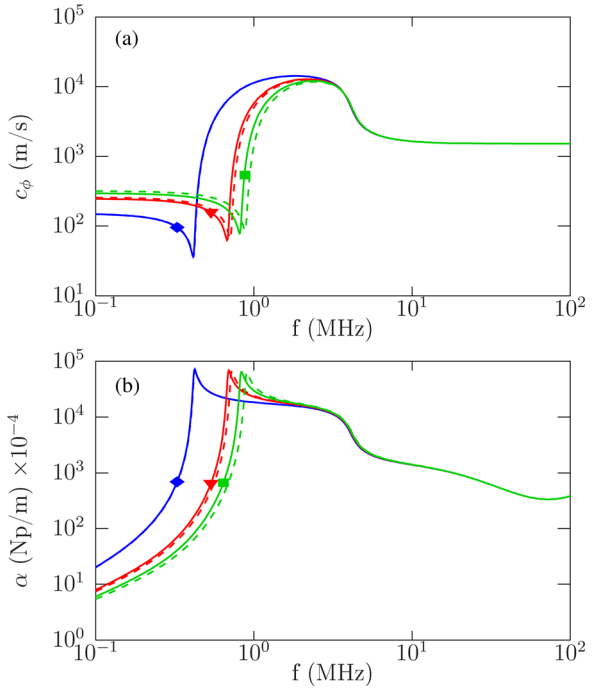

FIG. 8. (Color online) Sound velocity (a) and absorption coefficient (b) in a suspension of air-filled particles of size $R_{20} = 10$ μm. ◆: $G^s = 15$ MPa; ▼: $G^s = 88.8$ MPa; ■: $G^s = 150$ MPa. Solid/dashed lines: compressible/incompressible shell.

VII. CONCLUSION

Nanometric encapsulated droplets for medical therapy differ from standard ultrasound contrast agents by mainly two characteristics. First, because of their size and their production process, they generally present a thick shell, whose volume is on the order of magnitude of the volume of the inner droplet. Second, as their core is a liquid instead of a gas, the particle becomes much less compressible and the contrast of compressibility between the shell and the inner droplet is considerably reduced. In a previous study,[12] a model for dilute suspensions of nanodroplets has been proposed, which combines dilatational effects due to the radial motion of one single particle and translational motion relative to the continuous liquid phase. In the present paper, we proposed to extend this model by taking into account the effect of the shell compressibility and the polydispersity in size and shell thickness of the particles in the suspension. The compressible behavior of the shell is introduced in the equations governing the radial motion of the particle. The shell is thus modeled as a viscoelastic material, as well as the liquid core. Combining linear stress-strain relations with appropriate boundary conditions allows one to derive a system of two equations generalizing Rayleigh–Plesset equation for a compressible encapsulated viscoelastic sphere surrounded by a weakly compressible, Newtonian liquid. In the framework of the linear harmonic acoustic propagation, the compressibility induces an apparent "relaxing" behavior of the shell with a transition frequency f_{ch} which is almost the ratio of the viscosities over the elastic moduli, even though a standard rheological Kelvin–Voigt model is assumed for the shell material. Modifying the equations with a rheological Zener model tends to reduce the dispersion due to compressibility, depending on the value of the relaxation frequency f^s of the material relative to the transition frequency f_{ch}. The effect of shell compressibility on the dispersion and absorption curves is therefore quite straightforward, reducing the sound speed while increasing the absorption coefficient as a whole, and inducing strong dispersion of ultrasound waves as long as the transition frequency remains in the frequency range considered. The shell thickness is also a significant parameter, as the effect of the compressibility becomes stronger as the shell becomes larger relative to the volume of the inner core. On the other hand, little difference is observed between the monodisperse and polydisperse solutions, attesting that it is not the dominant effect inducing dispersion and absorption in suspensions of nanoparticles. Finally, it may be important to point out that, while the shell compressibility is of importance for nanometric liquid droplets, it has a minor effect for micrometric gaseous bubbles, for which the assumption of shell incompressibility remains valid. Future works will investigate from a theoretical point of view the influence of nonlinear shell elasticity. Experiments are in progress[27] and will be compared to the present model.

ACKNOWLEDGMENTS

This work was performed within the frame of Plan Cancer 2009–2013 (www.plan-cancer.gouv.fr), project NABUCCO (NAnometric Biocapsules for Ultrasonic triggering of anti-Cancer veCtOrized drug delivery) selected as a Research Project in Physics, Mathematics and Engineering Sciences Applied to Cancer Research. The authors are grateful to Dr. Nicolas Taulier (CNRS) and Professor Wladimir Urbach (Université Paris 5 René Descartes) from Laboratoire d'Imagerie Paramétrique (UMR UPMC CNRS 7623) for useful discussions.

[1]R. Challis, M. Povey, M. Mather, and K. Holmes, "Ultrasound techniques for characterizing colloidal dispersions," Rep. Prog. Phys. **68**, 1541–1637 (2005).
[2]P. S. Epstein and R. R. Carhart, "The absorption of sound in suspensions and emulsions. I. Waterfog in Air," J. Acoust. Soc. Am. **25**, 553–565 (1953).
[3]J. R. Allegra and S. A. Hawley, "Ultrasound techniques for characterizing colloidal dispersions," J. Acoust. Soc. Am. **51**, 1545–1564 (1972).
[4]M. Baudoin, J.-L. Thomas, F. Coulouvrat, and D. Lhuillier, "An extended coupled phase theory for the sound propagation in polydisperse concentrated suspensions of rigid particles," J. Acoust. Soc. Am. **121**, 3386–3397 (2007).
[5]L. L. Foldy, "The multiple scattering of waves. I. General theory of isotropic scattering by randomly distributed scatterers," Phys. Rev. **67**, 107–119 (1945).
[6]J. M. Evans and K. Attenborough, "Coupled phase theory for sound propagation in emulsions," J. Acoust. Soc. Am. **102**, 278–282 (1997).
[7]A. Doinikov and A. Bouakaz, "Review of shell models for contrast agent microbubbles," IEEE Trans. Ultrason. Ferroelectr. Freq. Control **58**, 981–993 (2011).
[8]N. Deshpande, A. Needles, and J. K. Willmann, "Molecular ultrasound imaging: current status and future directions," Clin. Radiol. **65**, 567–581 (2010).
[9]E. Pisani, N. Tsapis, J. Paris, V. Nicolas, L. Cattel, and E. Fattal, "Polymeric nano/microcapsules of liquid perfluorocarbons for ultrasonic imaging: physical characterization," Langmuir **22**, 4397–4402 (2006).

[10]O. Couture, P. D. Bevan, E. Cherin, K. Cheung, P. N. Burns, and F. S. Foster, "Investigating perfluorohexane particles with high frequency ultrasound," Ultrasound Med. Biol. **32**, 73–82 (2006).
[11]R. Diaz-Lopez, N. Tsapis, D. Libong, P. Chaminade, C. Conna, M. M. Chehimi, R. Berti, N. Taulier, W. Urbach, V. Nicolasa, and E. Fattal, "Phospholipid decoration of microcapsules containing perfluorooctyl bromide used as ultrasound contrast agents," Biomaterials **30**, 1462–1472 (2009).
[12]F. Coulouvrat, J.-L. Thomas, K. Astafyeva, N. Taulier, J.-M. Conoir, and W. Urbach, "A model for ultrasound absorption and dispersion in dilute suspensions of nanometric contrast agents," J. Acoust. Soc. Am. **132**, 3748–3759 (2012).
[13]C. C. Church, "The effects of an elastic solid surface layer on the radial pulsations of gas bubbles," J. Acoust. Soc. Am. **97**, 1510–1521 (1995).
[14]P. Mazur and D. Bedeaux, "A generalization of Faxén's theorem to nonsteady motion of a sphere through an incompressible fluid in an arbitrary flow," Physica **76**, 235–246 (1974).
[15]R. Gatignol, "The Faxén formulas for a rigid particle in an unsteady nonuniform Stokes-flow," J. Méc. Théor. Appl. **2**, 143–160 (1983).
[16]J. B. Keller and I. I. Kolodner, "Damping of underwater explosion bubble oscillations," J. Appl. Phys. **27**, 1152–1161 (1956).
[17]A. Prosperetti, "The equation of bubble dynamics in a compressible liquid," Phys. Fluids **30**, 3626–3628 (1987).
[18]E. A. Zabolotskaya, Y. A. Ilinskii, G. D. Meegan, and M. F. Hamilton, "Modifications of the equation for gas bubble dynamics in a soft elastic medium," J. Acoust. Soc. Am. **118**, 2173–2181 (2005).
[19]M. S. Plesset and D.-Y. Hsieh, "Theory of gas bubble dynamics in oscillating pressure fields," Phys. Fluids **3**, 882–892 (1960).
[20]A. S. Dukhin and P. J. Goetz, "Acoustic and Electroacoustic Spectroscopy," Langmuir **12**, 4336–4344 (1996).
[21]J. N. Marsh, C. S. Hall, S. A. Wickline, and G. M. Lanza, "Temperature dependence of acoustic impedance for specific fluorocarbon liquids," J. Acoust. Soc. Am. **112**, 2858–2862 (2002).
[22]N. G. Parker, M. L. Mather, S. P. Morgan, and M. J. W. Povey, "Longitudinal acoustic properties of poly(lactic acid) and poly(lactic-co-glycolic acid)," Biomed. Mater. **5**, 055004 (2010).
[23]K. Van de Velde and P. Kiekens, "Biopolymers: Overview of several properties and consequences on their applications," Polym. Test. **21**, 433–442 (2002).
[24]R. Christensen, *Theory of Viscoelasticity*, 2nd ed. (Dover, New York, 2003), pp. 15–20.
[25]K. W. Commander and A. Prosperetti, "Linear pressure waves in bubbly liquids: Comparison between theory and experiments," J. Acoust. Soc. Am. **85**, 732–746 (1989).
[26]M. Baudoin, J.-L. Thomas, F. Coulouvrat, and C. Chanéac, "Scattering of ultrasonic shock waves in suspensions of silica nanoparticles," J. Acoust. Soc. Am. **129**, 1209–1220 (2011).
[27]F. Coulouvrat, K. Astafyeva, J.-L. Thomas, N. Taulier, J.-M. Conoir, and W. Urbach, "Ultrasound characterization of mechanical properties of nanometric contrast agents with PLGA shell in suspension," in *Proceedings of the Acoustics 2012 Nantes Conference*, 23–27 April (2012), pp. 2539–2544.